## PAPER

# Selenium nanoparticles as antioxidants: green synthesis, characterization, and evaluation of bioactivity

Naila Qamar, [ID] *[a] Milka Poimala, [ID] [b,c] Jiri Jäntti, [ID] [b,c] Shuvashis Das Gupta, [ID] [a,d] Ayman Hawash, [ID] [e,f] Charith Sandipa Leelarathne, [ID] [e] Daniela Mennerich, [ID] [f,g] Antoine Dufour, [ID] [h] Janne T. A. Mäkelä, [ID] [b] Pirjo Åström [ID] †[e,f,i] and Mikko A. J. Finnilä [ID] †[a,f,i]

Selenium (Se), an important micronutrient with several biological effects, exhibits improved stability, biocompatibility, and safety through nanoparticle (NP) formulation. We present here a novel approach for producing smaller and structurally stable biogenic selenium nanoparticles (SeNPs) with bioactive coating. Poly(allylamine hydrochloride)-coated SeNPs were synthesized biogenically using *Trachyspermum ammi* (TA) seed extract, in parallel to chemically synthesized SeNPs. NPs were characterized and assessed for their *in vitro* antioxidant/radical scavenging potential through multiple complementary chemical assays along with the intracellular reactive oxygen species (ROS) scavenging and biocompatibility assay using human dermal fibroblasts. Both NPs were spherical and positively charged, with TA-SeNPs having a smaller size and a more amorphous nature. X-ray photoelectron spectroscopy confirmed the presence of elemental Se. Fourier transform infrared spectroscopy (FTIR) indicated the functional groups common to both NPs, with unique aliphatic, aromatic and glycosidic linkages, and phenolic compounds in TA-SeNPs, attributed to the TA extract. Both NPs showed dose-dependent antioxidative properties, with TA-SeNPs exhibiting significantly increased antioxidant activity among all the tested samples and showing similar to relatively higher activity relative to L-ascorbic acid (AA) and TA extract in several assays. Viability assays revealed that both NPs were nontoxic at low concentrations; however, cell viability is decreased at high concentrations, indicating dose-dependent cytotoxicity. TA-SeNPs suppressed reactive oxygen species more effectively at low concentrations, whereas SeNPs showed stronger activity at high concentrations. Our findings showed that the TA extract-mediated biosynthesis offers a cost-effective and biologically favorable route to produce SeNPs, with potential for safer antioxidant nanomedicine applications.

[a]*Research Unit of Health Science and Technology, Faculty of Medicine, University of Oulu, Oulu, FI-90014, Finland. E-mail: naila.qamar@oulu.fi*
[b]*Department of Technical Physics, University of Eastern Finland, Kuopio, 70211, Finland*
[c]*Diagnostic Imaging Center, Kuopio University Hospital, Wellbeing Services County of North Savo, Kuopio, Finland*
[d]*Department of Biomedical Engineering, Lund University, Lund, Sweden*
[e]*Research Unit of Biomedicine and Internal Medicine, Faculty of Medicine, University of Oulu, Oulu, FI-90014, Finland*
[f]*Biocenter Oulu, University of Oulu, Oulu, FI-90014, Finland*
[g]*Faculty of Biochemistry and Molecular Medicine, University of Oulu, Oulu, FI-90014, Finland*
[h]*Departments of Physiology and Pharmacology & Biochemistry and Molecular Biology, Cumming School of Medicine, University of Calgary, Calgary, AB T2N 4N1, Canada*
[i]*Infotech Oulu, University of Oulu, Oulu, Finland*
† These authors contributed equally to this work.

## 1. Introduction

Nanomedicine represents a field that applies nanomaterials to a broad range of medical applications, such as gene and drug delivery, medical imaging, diagnosis, biosensing, cancer therapy and wound dressings.[1] These medical applications, after their emergence in the mid-20th century, have driven key innovations across the fields of chemistry, physics, materials science, medicine, and biology.[2] The focus of nanoscience and nanotechnology is to design new materials with unique physicochemical properties resulting from the atomic and molecular rearrangements of the 1–100 nm scale.[3] This enables accurate manipulation of drug delivery systems at the nanoscale to achieve improved targeted drug delivery, controlled release, and enhanced pharmacokinetics while retaining essential drug activity. Various nanocarriers (polymeric nanoparticles [NPs], carbon nanomaterials, nanotubes, lipid-based systems, nanogels, liposomes and micelles) have been

developed that can be surface-functionalized to enhance cell penetration, immune compatibility, and receptor-mediated targeting of specific cells and tissues.[1] NP-based systems offer improved drug stability and prolonged shelf life, supplementing their clinical relevance.[3] Nanomaterials design and nanoscience integration continue to develop nanomedicine's translational potential, placing it as a main driver of future therapeutic strategies.[3,4]

Selenium (Se) is an important micronutrient exhibiting immunomodulation, anti-viral, anti-inflammatory, iodine metabolism,[5–7] antioxidant, antidiabetic, antiaging,[8] and tumor-suppressive properties.[5,6,8] Zero-valent selenium holds potent antioxidant activity and immune-modulating effects, and is non-toxic, making it a promising new source of selenium.[8] Selenium is the cofactor of thioredoxin reductases and glutathione peroxidases,[6,9] which can reduce oxidative stress-mediated tissue damage.[6,10] Several studies have shown that nano-selenium exhibits unique *in vivo* and *in vitro* antioxidant properties by activating selenoenzymes.[6] Selenium and its metabolites are incorporated into seleno-cysteine, recognized as the 21st amino acid, and form a key component of seleno-enzymes and seleno-proteins in biological tissues through a co-translational mechanism.[11] The absorption and systemic transport of microscale selenium are limited in the body,[8] which can hinder its biological efficacy. Nano-selenium formulations have been developed to improve bioavailability; however, these nanoscale forms also necessitate careful evaluation due to potential toxicity concerns.[10]

The high surface area-to-volume ratio of metal and metal oxide NPs of ~100 nm gives them unique properties compared to larger microparticles (~500 nm), enabling them to mimic antioxidant enzymes like superoxide dismutase and catalase. NPs regulate redox balance and release metal ions inside cells, exerting anti-oxidative and anti-inflammatory effects. These actions help break down reactive oxygen species (ROS), a term collectively used for the oxygen containing free radicals[12–14] generated by aerobic organisms because of normal physiological processes such as cell proliferation and differentiation, immune response,[12] metabolism, and cellular respiration. Thus, they play a pivotal role in many cellular signaling pathways,[12–14] *e.g.*, hydrogen peroxide ($H_2O_2$), superoxide anions ($O_2^-$), nitric oxide (NO), hypochlorite ions ($OCl^-$), and hydroxyl radicals ($OH^-$).[12,14] The antioxidant activity of a compound may be significantly indicated by its reducing power, related to the antioxidant potential of reductone to break the free radical chain with the donation of a hydrogen atom.[15]

Selenium nanoparticles (SeNPs) are more biocompatible and less toxic than their counterparts, selenite ($SeO_3^{2-}$) and selenate ($SeO_4^{2-}$).[16] The production and application of SeNPs have advanced significantly due to their numerous advantages, including chemical stability, biocompatibility, and low toxicity. The SeNPs have been synthesized by reduction techniques using glutathione, ascorbic acid and various reducing agents.[8] Many physical and chemical methods exist for NP production, but they often demand high energy and generate hazardous waste. Biogenic methods, in contrast, offer a green, eco-friendly, and cost-effective alternative.

SeNPs derived from bacteria, algae, and plants exhibit diverse biomedical applications, including antioxidant effects and anti-inflammatory, anti-arthritic, antimicrobial, immuno-modulatory and antiviral activities.[17–28] They efficiently scavenge the free radicals and enhance the endogenous antioxidant defense system (SOD, GPx, CAT, and GSH),[19–22,25,26] along with reducing the pro-inflammatory mediators and hindering arthritis progression in disease models.[27,28] SeNPs reveal potent anticancer properties *via* cell cycle arresting, ROS-mediated apoptosis induction, and selective cytotoxicity towards cancer cells with minimal toxicity to normal cells.[19,23,24] Furthermore, they have considerable antibacterial activity against *Escherichia coli* and *Staphylococcus aureus*,[19,20,25] antiviral effects against SARS-CoV-2,[18] and immunomodulatory effects with increased IgM, GSH, CAT, and lysozyme levels *in vivo*.[17]

"*Trachyspermum ammi*" (TA) generally known as "Ajwain" belongs to the Apiaceae family.[29,30] Phytochemical analysis has shown that TA contains a variety of constituents, including glycosides, carbohydrates, phenolic compounds, saponins, protein, fiber, fat, volatile oils (such as γ-terpinene, thymol, α- and β-pipene, and para-cymene), as well as minerals like phosphorus, calcium, nicotinic acid, and iron. Thymol, a biologically active compound present in TA, contributes to its antioxidant, anti-inflammatory, immunomodulatory,[29] anti-filarial, anti-microbial, anthelmintic,[31] and gastro-protective activities.[29]

TA is traditionally used to treat inflammatory and pain-related conditions although limited studies have been reported on its anti-inflammatory and antioxidant properties.[32] TA has recently gained interest beyond the traditional medicinal uses towards its emerging role in green nanotechnology. TA extract-derived NPs, including gold,[33] silver,[34] selenium,[28] nickel oxide[35] and zinc oxide,[36] exhibit broad biomedical activities such as anticancer, antioxidant,[37] antimicrobial, and wound healing effects.[35,37] Beyond biomedicine, TA-derived metal oxide NPs exhibit potential for wastewater treatment through photocatalytic pollutant degradation,[37] also used in agriculture *via* seedling growth and germination,[38] while TA-derived nano-emulsions are widely used in food packaging.[37]

The efficiency of TA-mediated biosynthesis is attributed to its phytochemical-rich composition, which plays a key role in both metal ion reduction and NP stabilization. Monoterpenes such as thymol and carvacrol assist in metal ion reduction, while tannins, terpenoids, flavonoids, and alkaloids act as natural capping agents, enhancing the colloidal stability and bioactivity of NPs. The multifunctionality of the TA extract highlights its suitability for sustainable NP synthesis.[37]

Previous studies have evaluated the effects of TA seed extract and SeNPs individually in arthritic models,[32,39] but their combined efficacy remains to be investigated. This study focused on the synthesis and characterization of SeNPs using both chemical and biogenic methods, including the green synthesis of TA-SeNPs using the TA seed extract. Their antioxidant

and radical scavenging properties were evaluated through multiple *in vitro* assays, along with preliminary biocompatibility assessments.

## 2. Materials and methods

### 2.1. Chemicals

Sodium selenite ($Na_2SeO_3$), L-ascorbic acid (AA), potassium ferricyanide, ferric chloride ($FeCl_3$), trichloroacetic acid (TCA), sodium nitroprusside, 2,2-diphenyl-1-picrylhydrazyl (DPPH), Dulbecco's modified Eagle's medium (DMEM; D5796), sodium pyruvate, penicillin/streptomycin, resazurin sodium salt, *tert*-butyl hydroperoxide solution, 2′,7′-dichlorofluorescein diacetate (DCFH-DA), and bovine serum albumin (BSA) (7.5%) in Dulbecco's phosphate-buffered saline (DPBS) were sourced from Sigma-Aldrich (St Louis, USA). Poly(allylamine hydrochloride) (PAH), pyrogallol, and fetal bovine serum (FBS) were obtained from Thermo Fisher Scientific (Dreieich, Germany), while trypsin-ethylenediaminetetraacetic acid (R7017) and hydrogen peroxide ($H_2O_2$) (30%) were sourced from Merck KGaA (Darmstadt, Germany).

### 2.2. Optimization of NP synthesis

Several concentrations of the precursor $Na_2SeO_3$ (10–40 mM), different ratios between the *Trachyspermum ammi* (TA) extract and the precursor (1 : 1–2 : 1 v/v) and reaction temperature (RT and 90 °C) were tested to determine the ideal reaction conditions for nanoparticle (NP) synthesis. The progression of NP synthesis and the selenium nanoparticle (SeNP) concentrations were monitored by spectrophotometric measurements to confirm the optimized parameters for SeNP biosynthesis.

### 2.3. NP synthesis and purification

**2.3.1. SeNP synthesis.** SeNPs were synthesized by the reduction of $Na_2SeO_3$ using L-ascorbic acid (AA) as the reducing agent and poly(allylamine hydrochloride) (PAH) as the stabilizing agent. 10 mM $Na_2SeO_3$ solution (100 mL) was prepared in Millipore Milli-Q water by stirring at room temperature (RT) for 30 min to begin the synthesis. 10 mL of AA (0.05 g mL$^{-1}$) and 2 mL of PAH (0.038 g mL$^{-1}$) were subsequently added dropwise to the reaction mixture and stirred under the same conditions for an additional hour (h). The color change of the reaction mixture from white to brick red initially confirmed the successful NP synthesis.

**2.3.2. TA-SeNP synthesis.** The TA extract was prepared by soaking TA seeds (6 g) in 100 mL of Millipore Milli-Q water and shaking them in a dark incubator at 160 rpm (40 °C) for 24 h to produce Biogenic TA-SeNPs. The mixture was centrifuged at 18 514g (4 °C) for 40 min, and the supernatant was then filtered by using a 0.45 μm pore size Whatman filter paper. 1 : 2 dilution of TA extract was then used to prepare 10 mM $Na_2SeO_3$ solution (150 mL) by stirring at reaction temperature (RT) for 1 h. The subsequent steps were the same as those outlined in the chemical synthesis (section 2.2.1).

The color shift from golden to brick red initially confirmed the SeNP synthesis. Ultraviolet (UV)–visible spectroscopy was carried out for both types of NPs and precursor solutions to further confirm the synthesis of SeNPs in the solution using a UV-Vis V-660 spectrophotometer (Jasco corporation, Tokyo, Japan), operating in the wavelength range of 200–800 nm.

**2.3.3. Purification of NPs.** Both types of NPs were purified by ultracentrifugation at 250 000g (4 °C) for 1 h. The collected pellet was washed three times by resuspending the pellet in Millipore Milli-Q water, followed by ultracentrifugation as described above and removal of the supernatant. The purified pellet was collected and placed in an incubator at 37 °C overnight. Recovered NPs were stored at RT in a dark environment for further use.

### 2.4. Characterization of NPs

The characterization of NPs was performed through a tandem of techniques after synthesis confirmation. Zeta potential and polydispersity index (PDI) were determined using dynamic light scattering (DLS) with a Zetasizer Nano ZS (Malvern Panalytical, Malvern, UK) to analyze the colloidal stability of NPs. The size, morphology, and elemental composition of the NPs were determined by TEM (JEOL JEM-2200FS EFTEM/STEM (Tokyo, Japan)) followed by elemental analysis *via* energy-dispersive X-ray spectroscopy (EDS) using a JEOL Dry SD100GV detector.

Fourier transform infrared (FTIR) spectroscopy was performed in the spectral range of 500–4000 cm$^{-1}$ using a Thermo Nicolet iS50 FTIR spectrophotometer (Waltham, Massachusetts, USA) to identify the functional groups present in the NPs. Surface analysis and analysis of Se allotropes and elemental valence states were further performed by XPS-speciation analysis using a Thermo Fisher Scientific ESCALAB 250Xi system (Waltham, MA, USA). XRD was used to clarify the nature of NPs by using a Bruker D8 VENTURE SCXRD X-ray diffractometer (Billerica, Massachusetts, USA) operated at 40 kV with a constant current of 135 mA, using Cu Kβ as the source of radiation over the scanning range of the Bragg angle 10–130°.

Furthermore, Raman microspectroscopy was performed on thin films and powder samples to study the crystallinity of the synthesized NPs. A Thermo Scientific DXRTM2xi confocal Raman imaging microscope (Waltham, Massachusetts, USA) equipped with a ×50/0.3 NA air objective was used for this purpose. Additionally, scanning area electron diffraction (SAED) was performed on the same previously described TEM samples, using a JEOL JEM-2200FS equipped with a TVIPS TemCam F416 (16 MP) to further validate the nature.

### 2.5. *In vitro* antioxidant/radical scavenging activities of NPs

The TA extract (control), TA-SeNPs, and SeNPs were assessed for their antioxidant/radical scavenging potentials through a panel of *in vitro* chemical assays, including ferric-reducing antioxidant power (FRAP) assay, DPPH radical scavenging activity, hydrogen peroxide ($H_2O_2$) scavenging properties, superoxide anion ($O_2^-$) scavenging potential, and nitric oxide

(NO) scavenging activity, in comparison with L-ascorbic acid (AA), a standard antioxidant. The absorbance was recorded by using a Bio-Rad SmartSpec™ 3000 spectrophotometer (Hercules, California, USA) after incubating the NPs with specific radical-generating systems at various concentrations. The percentage of inhibition/reducing capacity was then calculated.

### 2.6. Cell experiments for determining the cytocompatibility and antioxidant activity of NPs

**2.6.1. Resazurin-based viability assay.** Fibroblast cells were treated for viability assessments with the TA extract (control), TA-SeNPs, and SeNPs at various concentrations for 48 h and 72 h time intervals. Cytotoxicity was determined by using a resazurin assay, and the half maximal inhibitory ($IC_{50}$) values were calculated by using a four-parameter logistic model based on non-linear regression analysis.

**2.6.2. DCFH-DA-intracellular ROS assay.** A cell-based reactive oxygen species (ROS) scavenging assay (DCFH-DA) was performed using human dermal fibroblasts to determine the intracellular antioxidant effect of both NPs. Cells were treated with varying concentrations of NPs for 3 h with additional incubation with 500 μM $H_2O_2$ for 30 min. The ROS scavenging antioxidant potential of NPs was assessed by using the 2′,7′-dichlorofluorescein diacetate (DCFH-DA) fluorescent probe; the strength of the fluorescence signal reflects the amount of ROS present. The DCFH-DA-intracellular ROS assay was performed by the method previously described in ref. 40 with slight modifications.

The SI provides full experimental details, protocols, reagent concentrations, and calculation formulae.

### 2.7. Statistical analysis

OriginPro 2022b (OriginLab Corporation, Northampton, MA, USA) was utilized primarily for data visualization and the analysis of the characterization results; GraphPad Prism version 10 (GraphPad Software, San Diego, CA, USA) was used for statistical analysis and graph generation related to radical scavenging assays and cell experiments. Statistical comparisons were conducted using two-way ANOVA followed by Bonferroni's and Tukey's multiple comparison tests. Differences with $p < 0.05$ were considered statistically significant.

## 3. Results

### 3.1. Optimization of NP synthesis

Nanoparticle (NP) synthesis was optimized systematically by varying the $Na_2SeO_3$ concentration, temperature, and extract-to-precursor ratio, along with spectrophotometric monitoring of NP synthesis. Increasing precursor concentration and temperature led to high absorbance intensity, resulting in peak broadening and red shifts, indicative of particle aggregation. Among the tested conditions, the evaluated temperatures resulted in broader absorption profiles and increased agglomeration (Fig. S1A and B).

The optimized conditions (10 mM concentration of $Na_2SeO_3$ at reaction temperature (RT) with *Trachyspermum ammi* (TA) extract to precursor ratio of 1:2) constantly yielded stable TA-SeNPs with uniform optical features and produced stable NPs with a narrow size distribution, which was further confirmed by TEM, EDS, XRD, and XPS analyses (Fig. S1C and D).

### 3.2. Synthesis of NPs

Successful synthesis was first confirmed by the color change of the reaction mixture from colorless to brick red for SeNPs (Fig. S2A) and golden to brick red for TA-SeNPs (Fig. S2B). The UV–visible spectrum showed the sharp absorption peak of SeNPs at 265 nm and 263 nm for TA-SeNPs, which substantially differed from the spectrum of the TA extract and $Na_2SeO_3$, indicating the formation of the NPs (Fig. S2C).

### 3.3. Characterization of NPs

**3.3.1. Colloidal stability.** The zeta potential of the SeNPs and TA-SeNPs was found to be +34.5 ± 0.5 mV and +30.4 ± 0.5 mV, respectively (Fig. S2D). DLS was employed to analyze the stability of NPs over time through hydrodynamic size distributions and a more precise level of monodispersity in NP solutions over 3 days from 0 h to 72 h. The findings of *Z*-average showed that SeNPs and TA-SeNPs were stable and well-dispersed up to 48 h; however, TA-SeNPs showed signs of agglomeration at 72 h. The PDI was less than 1 for both NPs, indicating the monodispersity of the samples (Fig. 1C).

**3.3.2. Nanoparticle size and elemental composition.** JEOL JEM-2200FS EFTEM/STEM (TEM) micrographs revealed the spherical/irregular morphology of both NPs and were used to determine the average particle size by measuring their diameters. The resulting histogram displayed a narrow size distribution, and the average NP size of 109.2 ± 0.7 nm and 17.6 ± 0.2 nm was observed for SeNPs and TA-SeNPs, respectively, *via* Gaussian fitting (Fig. 1A and B). Energy-dispersive X-ray spectroscopy (EDS) spectra of both SeNPs and TA-SeNPs displayed a prominent Se peak at 1.379 keV, with mass percentages of 91.33% and 76.99%, respectively. SeNPs also showed peaks for silicon (Si, 3.88%) and oxygen (4.80%) (Fig. 2A). In contrast, TA-SeNPs exhibited additional peaks corresponding to nitrogen (N, 0.392 keV, 9.66%), oxygen (O, 0.525 keV, 11.76%), and silicon (Si, 1.739 keV, 1.59%) (Fig. 2B). Fig. S3A and B show the detailed EDS spectra with the representative KeV for SeNPs and TA-SeNPs, while Fig. 2C shows the detailed variations in the elemental composition of both NPs in terms of mass %.

**3.3.3. Functional group identification and speciation analysis of selenium.** Fourier transform infrared (FTIR) spectra of chemically synthesized SeNPs showed only one PAH-associated characteristic band of the C–H bond at 2653 cm$^{-1}$ shifted from 2866 cm$^{-1}$. Both NPs exhibited a peak corresponding to C–Cl stretching in the region of 532–542 cm$^{-1}$. In contrast, the spectral bands of the TA extract at 2925 cm$^{-1}$, 1561 cm$^{-1}$, 1407 cm$^{-1}$, 1021 cm$^{-1}$, and 650 cm$^{-1}$ were shifted to 2871 cm$^{-1}$, 1511 cm$^{-1}$, 1447 cm$^{-1}$, 1028 cm$^{-1}$, and 758 cm$^{-1}$ in TA-SeNPs, which could be assigned to aliphatic C–H, aro-
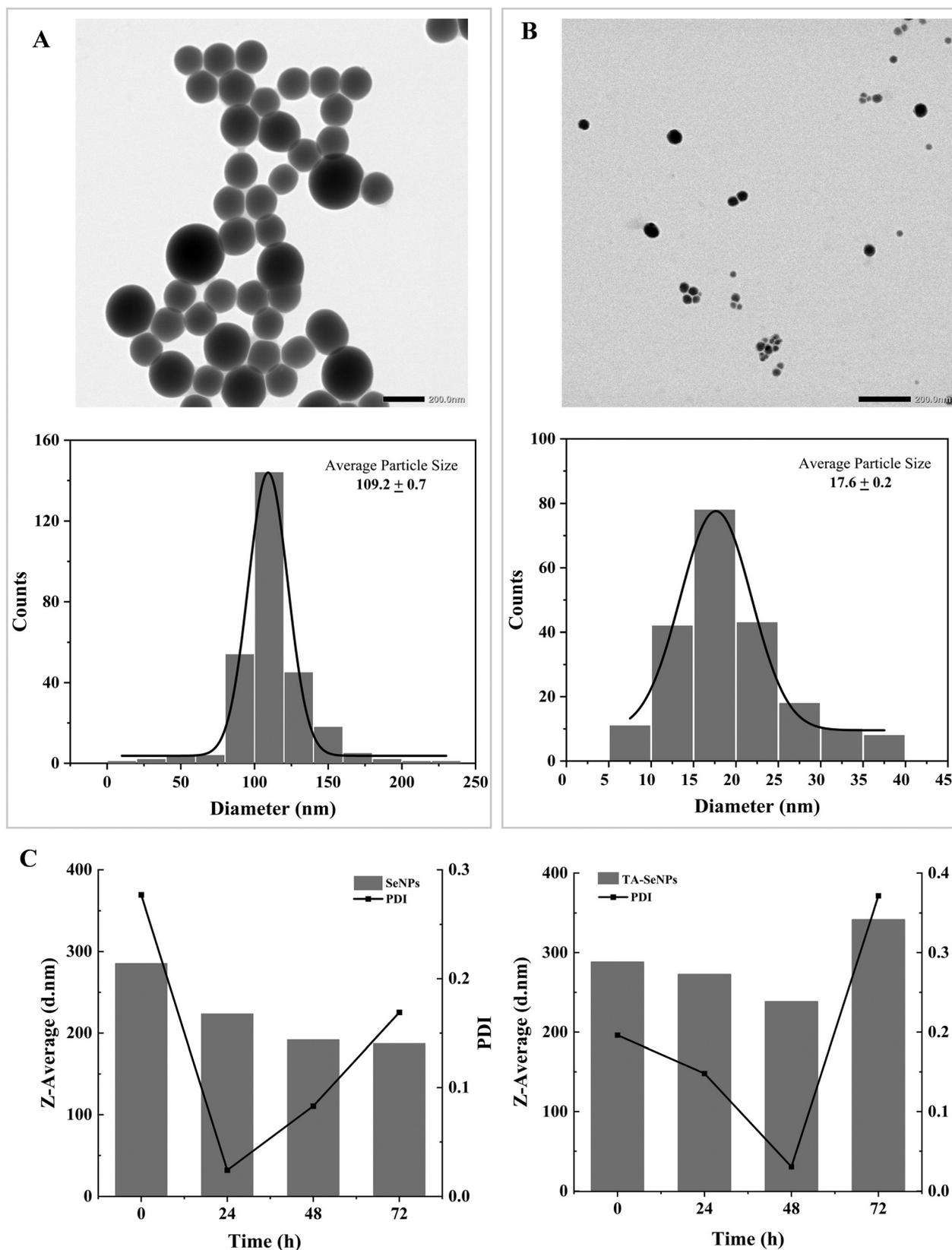
**Fig. 1** Transmission emission microscopy (TEM) micrographs of both NPs and their related size distribution histogram obtained from TEM analysis. The solid line corresponds to the Gaussian fitting used to determine the average particle diameter. TEM images showing the spherical/irregular morphologies and size histogram with the calculated sizes (mean ± standard deviation) for (A) selenium nanoparticles (SeNPs) and (B) *Trachyspermum ammi* (TA)-SeNPs. (C) Stability of nanoparticles (NPs) assessed by the *Z*-average particle size and polydispersity index (PDI) measured at different time intervals from 0–72 h indicating changes in NP size distribution and dispersion uniformity over time, reflecting colloidal stability.
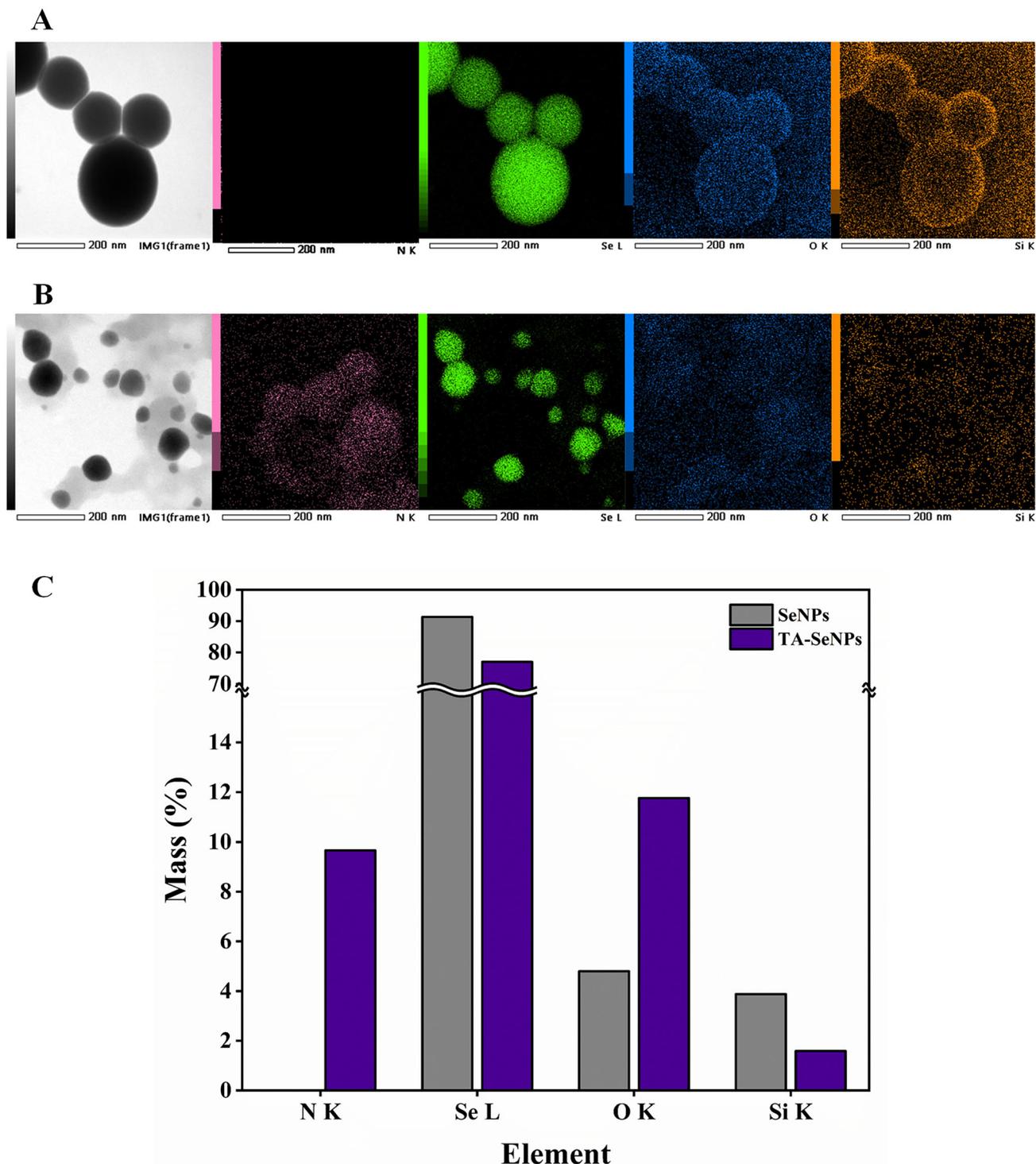
Fig. 2 Energy-dispersive X-ray spectroscopy (EDS). (A) Elemental mapping of selenium nanoparticles (SeNPs) and (B) *Trachyspermum ammi* (TA)-SeNPs, showing the elemental distribution and confirming the presence of selenium in both nanoparticle samples, and (C) the mass percentage (%) spectra of the elements present in both NPs.

matic C=C, phenolic and glycosidic C–O, and aromatic C–H bending, respectively. The PAH spectral bands at 2866 cm$^{-1}$, 1500 cm$^{-1}$, and 997 cm$^{-1}$ were shifted to 2871 cm$^{-1}$, 1511 cm$^{-1}$, and 842 cm$^{-1}$ in TA-SeNPs, corresponding to C–H (aromatic rings), N–H, and C–N (amines) bonds. These indicate effective surface functionalization of TA-SeNPs with both TA extract and poly(allylamine hydrochloride) (PAH) (Fig. 3A). Table S1 shows the TA extract-derived functional groups identi-
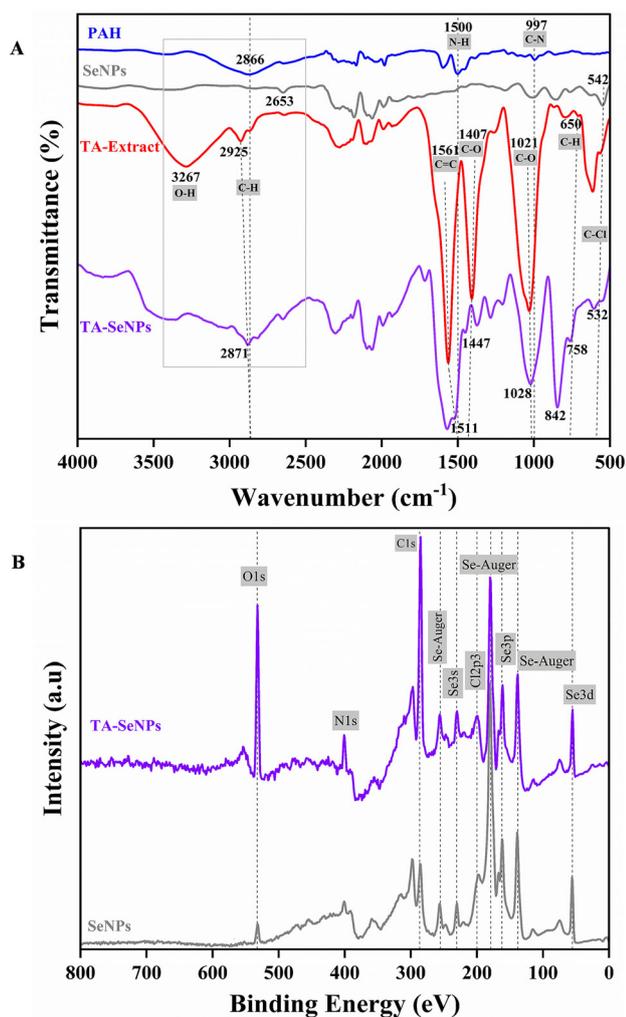
**Fig. 3** (A) Fourier-transform infrared (FTIR) spectra of poly(allylamine hydrochloride) (PAH), selenium nanoparticles (SeNPs), the *Trachyspermum ammi* (TA) extract, and TA-SeNPs showing the characteristic functional groups and confirming the interactions between components during NP synthesis. (B) X-ray photoelectron spectroscopy analysis of both biogenic nanoparticles showing the elemental composition and surface functional groups.

fied in the FTIR spectrum of TA-SeNPs along with their detailed involvement in biosynthesis.

XPS was performed for speciation analysis of Se, and prominent surface peaks were observed at 529.48 eV (O 1s), 285.07 eV (C 1s), and 199.44 eV (Cl 2p3) for both types of SeNPs in the spectra. The N 1s peak at 399.44 eV was notably absent in chemically synthesized SeNPs, indicating differences in surface composition. Se peaks were detected at 55.03 eV (Se $3d_{5/2}$), 161.5 eV (Se $3p_{3/2}$), and 230.03 eV (Se 3s), consistent with zero-valent selenium ($Se^0$). Additional Auger peaks were observed at 138.6 eV, 180.03 eV, and 256.52 eV in both samples, corresponding to elemental selenium (Fig. 3B).

**3.3.4. Crystallinity of NPs.** The XRD diffractogram of chemically synthesized SeNPs was consistent with the standard hexagonal selenium reference (International Centre for

Diffraction Data (ICDD) card no. 04-002-1257). The diffraction pattern exhibits peaks at $2\theta$ values of 27°, 35°, 51°, 53°, 61°, 66°, 73°, and 112° could be indexed to the (100), (101), (110), (012), (201), (003), (022), (210), and (123) planes, respectively. The spectrum of Ta-SeNPs revealed no dominant diffraction peak, indicating its amorphous nature (Fig. 4A). Raman spectra of TA-SeNPs showed a distinctive peak of amorphous Se (a-Se) at 252 cm$^{-1}$, corresponding to the A1 stretch of the Se–Se mode of vibrations, along with the shoulder peak at a lower wavenumber (238 cm$^{-1}$) attributed to the molecular selenium (Se8) embedded mainly within the amorphous Se matrix. SeNPs showed sharp characteristic peaks at 141 cm$^{-1}$ and 237 cm$^{-1}$, attributed to the E and A1 modes of trigonal Se (t-Se) (Fig. 4B). The results of XRD and Raman spectroscopy were further confirmed by the scanning area electron diffraction (SAED) patterns, which indicated the amorphous nature of TA-SeNPs, and the nanocrystalline phases of selenium in chemically synthesized SeNPs (Fig. 5A).
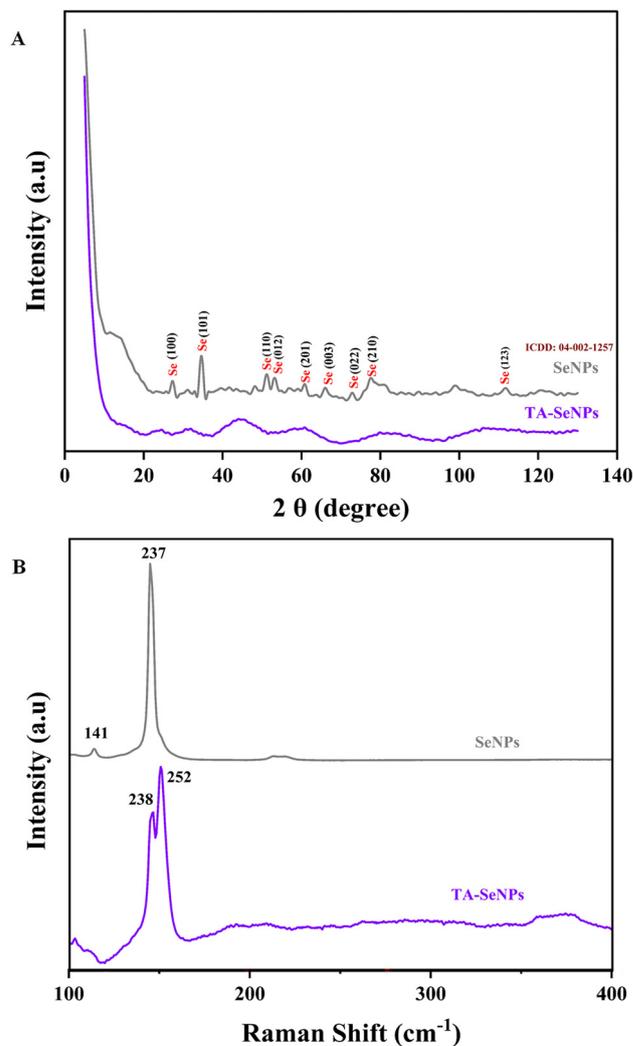


**Fig. 4** (A) X-ray diffractometry diffractogram (XRD) and (B) Raman spectra of the chemically synthesized selenium nanoparticles (SeNPs) and *Trachyspermum ammi* (TA)-SeNPs.
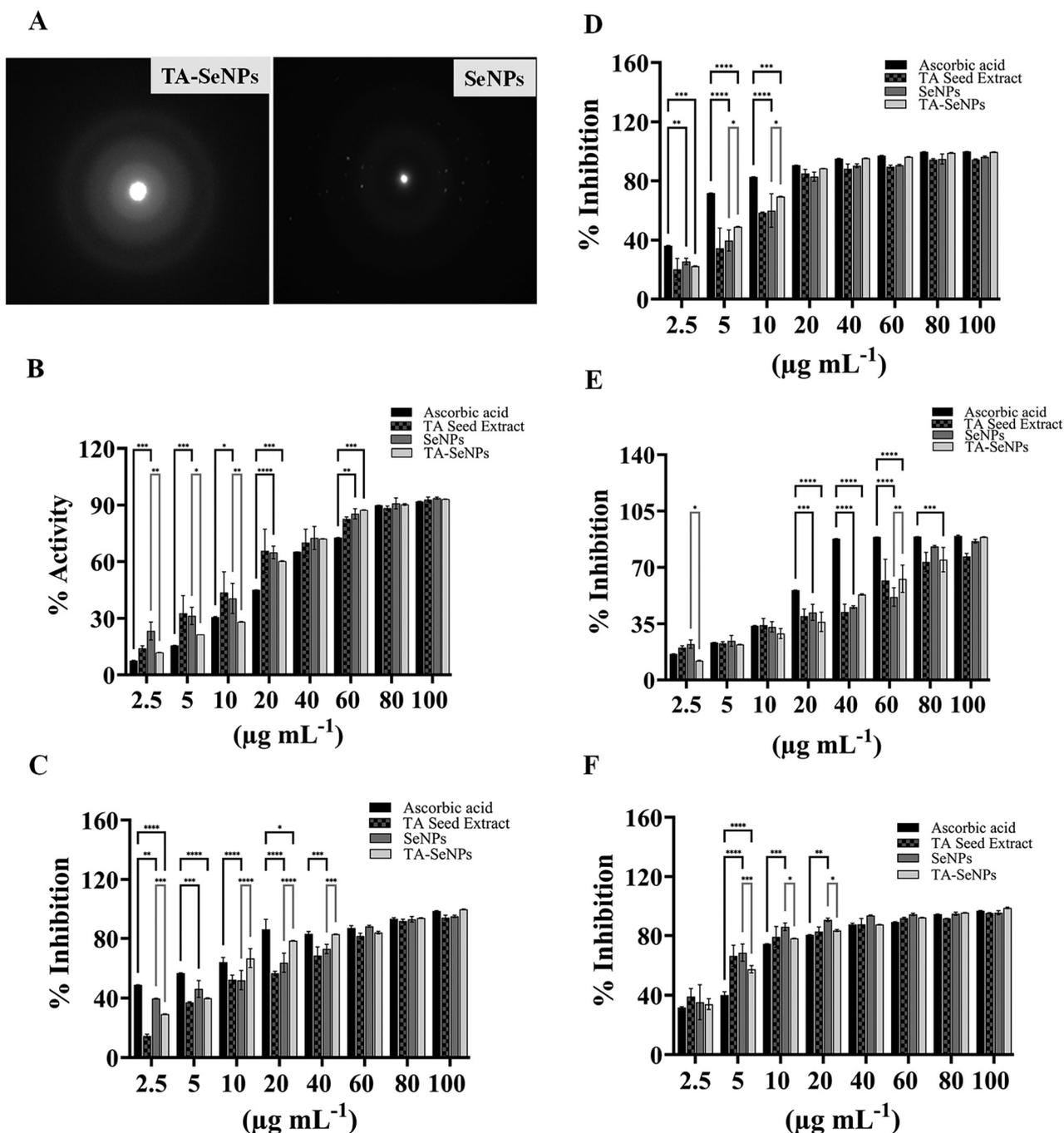
**Fig. 5** (A) The scanning area electron diffraction (SAED) pattern. Antioxidant/radical scavenging activities of ascorbic acid (control), the *Trachyspermum ammi* (TA) seed extract (control), selenium nanoparticles (SeNPs), and TA-SeNPs *in vitro*, (B) ferric reducing antioxidant power (FRAP) assay, (C) 2,2-diphenyl-1-picrylhydrazyl (DPPH) assay, (D) hydrogen peroxide ($H_2O_2$) scavenging assay, (E) superoxide ($O_2^-$) scavenging assay, and (F) nitric oxide (NO) scavenging assay. The results are presented as the mean $\pm$ standard deviation ($n = 3$). Statistical analysis: two-way ANOVA followed by Tukey's *t*-test; (*$p < 0.05$, **$p < 0.01$, ***$p < 0.001$ and ****$p < 0.0001$).

## 3.4. Evaluation of the antioxidant/radical scavenging activities of NPs

Multiple chemical assays on TA-SeNPs and SeNPs (FRAP, DPPH, $H_2O_2$, $O_2^-$, and NO scavenging activities) were performed in comparison with AA (standard antioxidant) to assess the *in vitro* antioxidant activity of the TA extract (control) (Table S2).

FRAP increased constantly when the concentrations of the tested compounds were increased, suggesting their dose-dependent response. SeNPs and the TA extract exhibited significantly better reducing power than AA and TA-SeNPs at

lower doses of 2.5 and 5 μg mL⁻¹ (Fig. 5B). However, TA-SeNPs exhibited significantly higher reducing power over all other tested compounds at higher concentrations of 40–100 μg mL⁻¹.

Both NPs showed significantly better DPPH radical scavenging activity compared to AA. TA-SeNPs exhibited greater DPPH radical scavenging activity compared to chemically produced SeNPs and the TA extract, with their activity at 100 μg mL⁻¹ surpassing that of AA. However, the radical scavenging activity was found to be more than 90% at higher doses of all tested compounds (Fig. 5C).

A dose-dependent increase in $H_2O_2$ radical scavenging activities was observed for all tested compounds. AA exhibited a plateau in response at 80 and 100 μg mL⁻¹, while the TA extract showed a slight decrease in response at 100 μg mL⁻¹ (Fig. 5D).
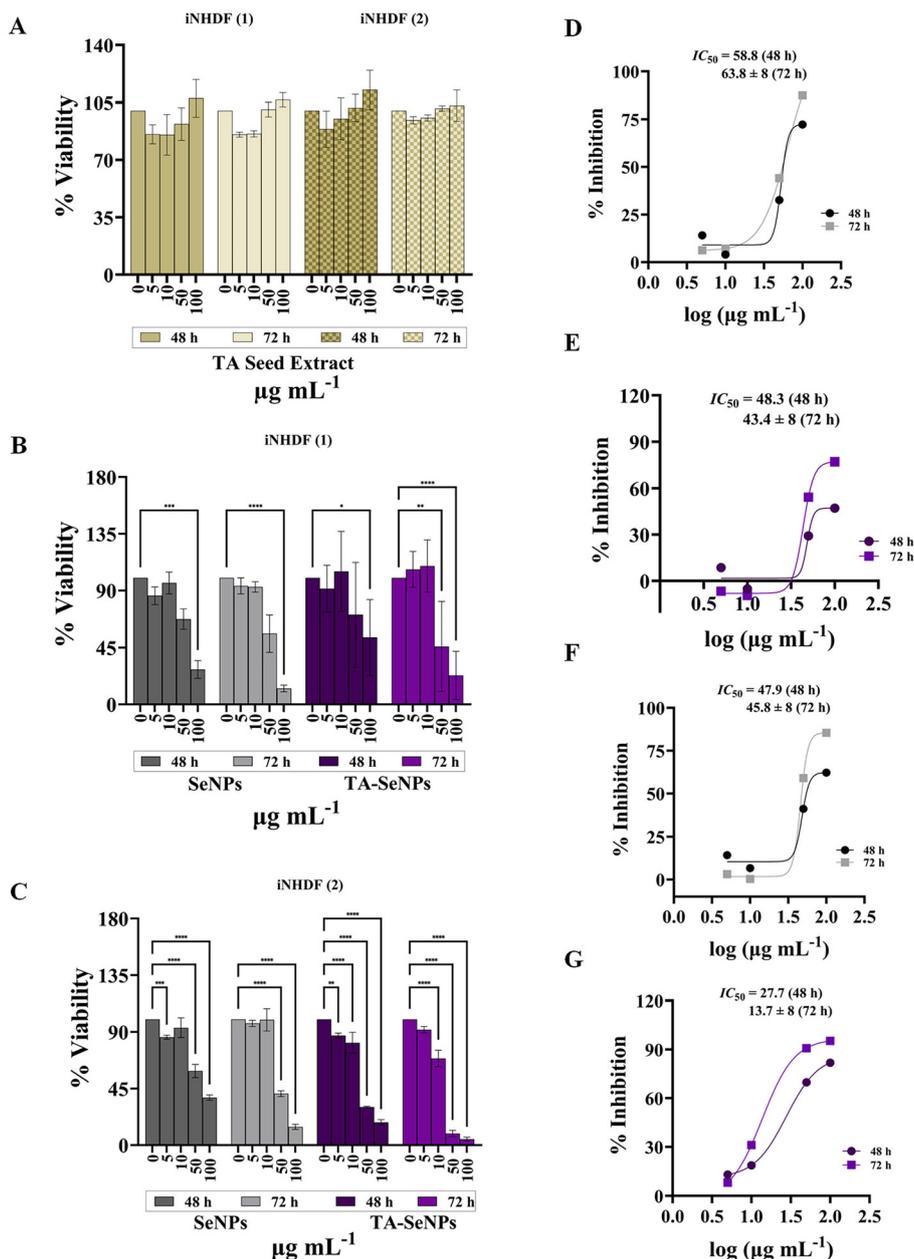


**Fig. 6** Biocompatibility of the nanoparticles (NPs) and TA extract (control) on human dermal fibroblast cells (iNHDF) through cell viability: (A) TA extract, (B) iNHDF-1 and (C) iNHDF-2. The values are presented as the percentage of reduction compared to the untreated cells, set at 100%. The results are presented as the mean ± standard deviation of three independent experiments. Statistical analysis: over time intervals of 48, and 72 h *$P <$ 0.05, **$P <$ 0.01, ***$P <$ 0.001 and ****$P <$ 0.0001. Half maximal inhibitory concentration ($IC_{50}$) values for iNHDF-1 – (D) selenium nanoparticles (SeNPs) and (E) *Trachyspermum ammi* (TA)-SeNPs and for iNHDF-2 – (F) SeNPs and (G) TA-SeNPs after 48 and 72 h of exposure, indicating comparative cytotoxicity and time-dependent effects.
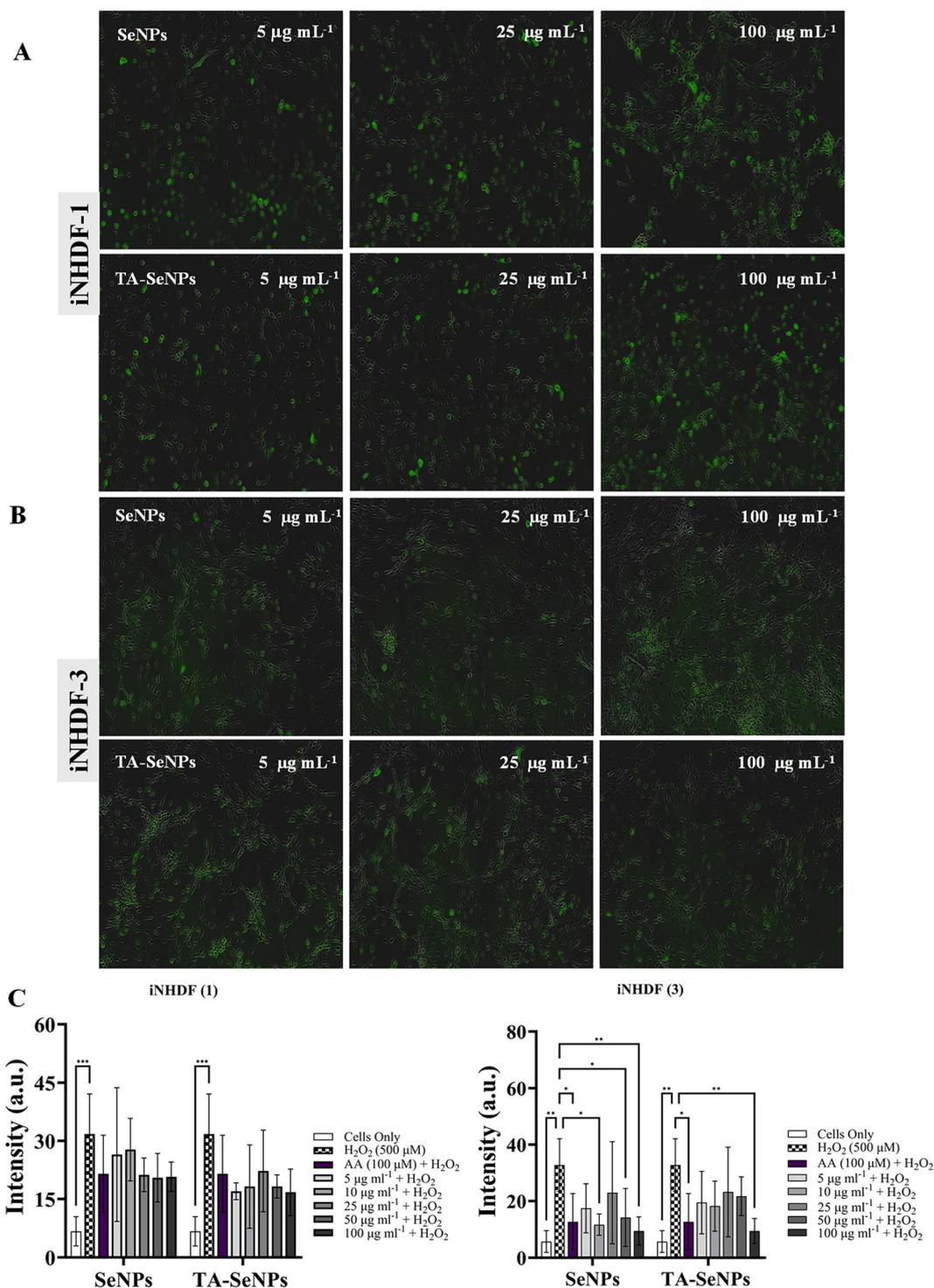
**Fig. 7** Reactive oxygen species (ROS) scavenging activity of the nanoparticles on human dermal fibroblast cells determined through the 2′,7′-dichlorofluorescein diacetate (DCFH-DA) assay. Selenium nanoparticles (SeNPs) and *Trachyspermum ammi* (TA)-SeNPs + hydrogen peroxide ($H_2O_2$) treated (A) iNHDF-1 cells and (B) iNHDF-3 cells; (C) the values are presented as the percentage of reduction compared to $H_2O_2$-treated cells, a positive control. Ascorbic acid (AA) + $H_2O_2$-treated cells served as the controls. The results are presented as the mean $\pm$ SD of four technical repeats of experiments. Statistical analysis: two-way ANOVA followed by the Bonferroni *post-hoc* test; (*$p < 0.05$, **$p < 0.01$, ***$p < 0.001$ and ****$p < 0.0001$). Magnification: ×10 and the scalebar is 200 μm for all images.

All the tested concentrations of NPs, TA extract, and AA showed an increasing trend in inhibiting the superoxide anion radicals. However, the response plateaued for AA at doses of 60, 80, and 100 μg mL$^{-1}$. A dose-dependent response was observed for both NPs; however, their overall activity was significantly lower than the standard (Fig. 5E).

The dose-dependent increasing trend was observed in the NO radical scavenging activities of all the tested compounds, with the highest activity of 99.16% at the concentration of 100 μg mL$^{-1}$ of both NPs. Both NPs and TA extract showed significantly higher activity than that of AA (Fig. 5F).

### 3.5. Effect of NPs on cell viability

Treatment with TA extract did not significantly affect the cell viability of either iNHDF-1 or iNHDF-2 cell lines at either 48 h or at 72 h (Fig. 6A). Treatment with SeNPs for 48 h at concentrations of 5, 50, and 100 μg mL$^{-1}$ significantly reduced the cell viability in iNHDF-2 cells to 86%, 59%, and 38% respectively, while it was reduced to 28% with 100 μg mL$^{-1}$ in iNHDF-1 cells. After 72 h, 100 μg mL$^{-1}$ SeNPs reduced the cell viability to 13% in iNHDF-1 and 15% in iNHDF-2 compared to the control group (100%). In contrast, TA-SeNP treatment for 48 h reduced the viability of iNHDF-2 cells to 87%, 81%, 30%, and 18% at the concentrations of 5, 10, 50, and 100 μg mL$^{-1}$, respectively. 100 μg mL$^{-1}$ reduced the viability to 53% in iNHDF-1 cells. The viability of iNHDF-2 was further reduced to 69% with 10 μg mL$^{-1}$, 9% with 50 μg mL$^{-1}$, and 5% with 100 μg mL$^{-1}$ after 72 h of exposure. It was reduced to 46% and 23% with 50 μg mL$^{-1}$ and 100 μg mL$^{-1}$ in iNHDF-1 cells (Fig. 6B and C).

A time-dependent decreasing trend was observed in the case of exposure of both NPs, with significant differences noticed between all concentrations and controls over different time intervals.

The IC$_{50}$ values of TA-SeNPs and SeNPs against both iNHDF cell lines were determined at 48 and 72 h. The IC$_{50}$ values of TA-SeNPs against iNHDF-1 and 2 were 48.3 μg mL$^{-1}$ and 27.7 μg mL$^{-1}$ at 48 h and these further decreased to 43.4 μg mL$^{-1}$ and 13.7 μg mL$^{-1}$ after 72 h of exposure. SeNPs showed IC$_{50}$ values of 58.8 μg mL$^{-1}$ and 47.9 μg mL$^{-1}$ at 48 h and were 63.8 μg ml$^{-1}$ and 45.8 μg mL$^{-1}$ after 72 h, indicating time-dependent cytotoxicity (Fig. 6D–G).

### 3.6. ROS scavenging effects of NPs

H$_2$O$_2$ was applied as a positive control to stimulate oxidative stress, and higher intracellular ROS levels were observed compared to untreated cells as indicated by the 2′,7′-dichlorofluorescein diacetate (DCFH-DA) assay. Fig. 7A and B present the microscopy images for 5, 25 and 100 μg mL$^{-1}$ for both cell lines (all concentrations in Fig S4 and S5). AA treatment significantly reduced oxidative stress. In contrast, the cells treated with chemically produced SeNPs showed a strong antioxidant response at higher concentrations of 25, 50, and 100 μg mL$^{-1}$ in iNHDF-1 cells, while significant ROS reduction was observed in iNHDF-3 cells at the concentrations of 10, 50 and 100 μg mL$^{-1}$, evidenced by a reduced fluorescence signal. The

TA-SeNP-treated cells displayed a strong antioxidant response, indicated by the reduced fluorescence intensity, with lower concentrations (5 and 10 μg mL$^{-1}$) being more effective at suppressing ROS than the higher concentrations in iNHDF-1 cells, while 10, 50 and 100 μg mL$^{-1}$ showed a significant reduction in the iNHDF-3 cells (Fig. 7C).

## 4. Discussion

Elemental Se (Se$^0$) has emerged as a functional biomaterial due to its low toxicity and multi-functional properties. Natural biological reduction of Se oxyanions (selenite and selenate) to Se$^0$ enables the biosynthesis of SeNPs using plants and microorganisms, offering a sustainable alternative to conventional synthesis methods (Table S3).[7,41] Bio-based systems are specifically suitable for this purpose, because microorganisms and plants simultaneously facilitate Se reduction and surface functionalization without any hazardous chemicals, yielding stable nanoparticles (NPs) with bio-active compounds on their surface.[7,42] We present here a unique and simple method that is safe and straightforward to produce small, stable, positively charged, amorphous SeNPs using seed extract. This synthesis method is unique due to its sequential biogenic–synthetic approach for producing small, stable NPs with preserved bioactivity. It combines TA extract-mediated nucleation, delayed AA addition to control the growth, and dual capping with plant-derived phytochemicals and synthetic poly(allylamine hydrochloride) (PAH), offering a broadly applicable NP synthesis strategy.

The shape, size, and composition of NPs can improve their sensitivity and selectivity, enabling their use in diverse industrial, biomedical, and environmental applications.[43] The synthesis of NPs was evaluated by adjusting precursor (Na$_2$SeO$_3$) and AA concentrations, TA-extract ratios and reaction temperature (RT). Among the tested conditions, 10 mM concentration of Na$_2$SeO$_3$ at RT constantly yielded stable SeNPs with uniform optical features, whereas the evaluated temperatures resulted in broader absorption profiles and increased agglomeration. The optimized synthesis was reproducible across three independent batches, generating NPs with consistent morphologies and UV spectra. The average yield of purified NP powder was 70–80 mg per 100 mL of the reaction mixture.

The improved stability of TA-SeNPs at RT may be attributed to controlled reduction kinetics and preservation of TA extract-derived bioactive phytochemicals that contribute to NP stabilization. The moderate, aqueous, and ambient reaction conditions highlight the scalability of this newly optimized TA-mediated biogenic synthesis approach for SeNP production.

A simple way to confirm synthesis is a brick red color change. The SeNP formation in both the chemical and biogenic systems was further confirmed by UV–visible spectral analysis (surface plasmon resonance). The precursor Na$_2$SeO$_3$ showed no visible absorption peak, indicating the absence of NPs, while the TA extract showed a broad absorption band with the maximum at 350 nm. The overlapping electronic tran-

sitions of various phytochemicals present in the TA extract could contribute to this broad absorption band. In contrast, both synthesized SeNPs and TA-SeNPs exhibited new different absorption peaks, reflecting the successful reduction of $SeO_3^{2-}$ to $Se^0$ and NP formation. The adsorption of plant biomolecules and dual capping with PAH further influenced the position and shape of the TA-SeNP absorption peak by modifying the electronic environment and could contribute to the minor red/blue shifts. Subsequent TEM and DLS analyses further confirmed their size distribution and dispersion. These findings were consistent with the previous research.[44,45]

TA-SeNPs have an additional coating of biomolecules attributed to the TA extract, which can interact with $Na_2SeO_3$ to control the growth of particles, resulting in the small spherical shape of NPs. The capping agents can depict a biological function to the particle that can be used to modify their therapeutic potential.[10] The stabilization of NPs by coating them with polymer or surface layers of biomolecules (phytocapping substances) is highly important to avoid agglomeration and can also aid in the reduction of precursor substances to produce NPs.[10] The PDI, hydrodynamic size, and zeta potential measurements are the indicators of size heterogeneity of NPs and are commonly used to assess their stability.[10,46] Both NPs were monodispersed with minimal agglomeration in SeNPs, while TA-SeNPs showed signs of agglomeration at 72 h.

XPS is commonly used to analyze the valency of elements and the bonding mechanisms with respect to their bonding energies.[45] The core elemental peaks of selenium represent Se $3d_{5/2}$, Se $3p_{3/2}$, and Se 3s, consistent with zero-valent selenium ($Se^0$). Additionally, Se Auger peaks supported the presence of zero-valent selenium. The absence of the characteristic $Na_2SeO_3$ peak at 59.1 eV further confirmed the complete reduction of selenite and successful SeNP synthesis. These XPS findings together confirmed that selenium in the synthesized NPs predominantly exists in the zero-oxidation state, characteristic of both biogenic and chemical SeNPs. The results were in line with the findings from previous studies.[45,46]

The analysis of the elemental composition through energy-dispersive X-ray spectroscopy (EDS) confirmed the presence of Se by its characteristic peak at 1.379 keV. Additional peaks of C, O and N indicate the presence of organic materials in the NP coatings. Nitrogen was notably absent in the spectrum of the chemically synthesized SeNPs, suggesting differences in the surface composition between the two types. A relatively high mass % of Se in the EDS spectrum could be attributed to the dominance of Se (high molecular weight) core and characteristic EDS detection limitations. The thin surface coatings were primarily composed of light elements (C, O, N, and H), of which hydrogen was undetectable while the other elements were detected with relatively low sensitivity, resulting in the comparatively high Se signal. These results suggested biomolecular capping on TA-SeNPs, consistent with previous studies.[42,46]

Plant-derived phytochemicals serve as the main contributors of SeNP synthesis due to their involvement in the natural reduction and surface functionalization processes, and they exhibit strong antioxidant, anti-inflammatory and epigenetic regulatory activities. Flavonoids, phenolics, terpenoids, alkaloids, and organosulfur compounds are the major classes of phytochemicals that can effectively scavenge the reactive oxygen species (ROS) and modulate key signaling pathways of cells, including Nef2, NF-κB, MAPKs, and PI3K/Akt. Surface functionalization of SeNPs with these compounds enhance colloidal stability and reduce agglomeration, and may improve biological efficacy with minimized toxicity, positioning the phytochemical-coated SeNPs as promising candidates for next-generation biomaterials.[47]

The presence of surface-bound biomolecules in NPs is further supported by the Fourier transform infrared spectroscopy (FTIR) analysis. FTIR analysis of the chemically synthesized SeNPs showed only one peak at 2653 cm$^{-1}$, attributed to the C–H stretch of an alkane from PAH, likely due to the low concentration of surface stabilizers. In contrast, the observed FTIR shifts in the TA-SeNP spectrum presented various bioactive compounds from the TA extract contributing to both the formation and stabilization of NPs. The presence of C–H aliphatic, C=C aromatic, C–O phenolic, and aromatic C–H bending suggests the involvement of major monoterpenes (thymol and carvacrol) which can involve in electron donation to accelerate the $SeO_3^{2-}/SeO_4^{2-}$ reduction and initiate the NP nucleation.[37,48] Thymol, a biologically active compound present in TA, contributes to its antioxidant, anti-inflammatory, and immunomodulatory properties.[30] Hence, the coating can be used to modulate the biological activity of NPs. Furthermore, the sharp peak corresponded to the C–H stretch of aliphatic –CH$_2$ and –CH$_3$ in the triterpenoid backbone of saponins, and the C=C bond confirmed the structure of the aglycone of saponins, along with a distinct band of the C–O bond indicating the glycosidic linkages, verifying the carbohydrate moieties on the surface of TA-SeNPs. These peaks altogether indicated the successful absorption of saponins on the surface of TA-SeNPs, serving as a natural capping and stabilizing agent during synthesis.[49] Saponins and flavonoids from the TA extract possibly interacted with selenium ions through the hydroxyl and glycosidic groups, forming the capping layer by metal chelation which prevented aggregation.[37] The shifted bands of amines (N–H and C–N) revealed PAH contribution as a stabilizing polymer, forming a dual capping layer with the plant biomolecules. This dual-capping layer of phytochemicals and PAH present synergistic reduction, stabilization and surface functionalization of TA-SeNPs with enhanced colloidal stability and biocompatibility. The findings align with previous reports[43,50–53] and highlight the functional versatility imparted by green synthesis approaches.

The X-ray diffractogram obtained for the chemically produced SeNPs showed the nanocrystalline planes of Se, consistent with the standard hexagonal selenium, consistent with the literature.[54] In contrast, TA-SeNPs lacked sharp and clear peaks, indicating their amorphous nature. Similar findings have been published for *Yarrowia lipolytica*-produced SeNPs.[42] This observation was consistent with prior reports on biogenic

SeNPs, including those produced by *Pseudomonas aeruginosa* ATCC 27853,[55] *Bacillus mycoides* SeITE01[56] and *Lactobacillus casei* ATCC 393.[57] The Raman spectra of SeNPs exhibited two distinct peaks of t-Se in agreement with the spectra reported in earlier studies.[58–61] In contrast, the coexistence of the broad amorphous peak with the $Se_8$ shoulder in the spectra of TA-SeNPs suggested molecular clustering within the amorphous matrix of NPs. The results aligned with previous studies that reported a shoulder peak at 235 cm$^{-1}$, along with the prominent peak of a-Se at 250 cm$^{-1}$.[45,58,62] Furthermore, scanning area electron diffraction (SAED) confirmed the amorphous nature of TA-SeNPs.

The antioxidant activity of a compound may be significantly indicated by its reducing power, related to the antioxidant potential of reductone to break the free radical chain with the donation of a hydrogen atom.[15] A comprehensive evaluation of the antioxidant activity of both NPs was performed through multiple complementary *in vitro* chemical assays (FRAP, DPPH, $H_2O_2$, superoxide, and NO scavenging assays) along with the intracellular ROS scavenging assay (DCFH-DA) using human dermal fibroblasts. TA extract served as a biological control, whereas L-ascorbic acid (AA) served as a standard antioxidant control in both chemical and cell-based assays.

TA-SeNPs showed improved reducing power compared to SeNPs, potentially due to the presence of phytoconstituents like steroidal saponins (that also have electron-donating antioxidant capacity) in the extract.[15] Both NPs showed a dose-dependent increasing trend in response to all tested parameters, with the highest response observed in the DPPH assay and NO radical scavenging activities, like in previous reports.[63–65]

The free radical precursors, superoxide anions, can be produced *in vivo*, resulting in the formation of $H_2O_2$ through a dismutation reaction.[15,66] Both NPs and TA extract exhibited dose-dependent antioxidant activity. However, their overall scavenging efficiency was slightly lower than that of AA. Similar efficacy has been reported previously for Murraya koenigii (Mk) extract-derived Mk-SeNPs.[67] Furthermore, our data also indicated that biogenic TA-SeNPs showed comparatively better antioxidant activity than the chemically produced SeNPs among all the tested samples and showed similar-to-higher activity relative to AA and the TA extract in several assays, aligning with the reports.[68]

Selenium compounds exhibited the lowest toxicity in their elemental $Se^0$ form, making them promising agents to combat many diseases. The reduction of $SeO_3^{2-}/SeO_4^{2-}$ to $Se^0$ represents a key mechanism for selenium oxyanion detoxification under aerobic and anaerobic conditions.[7] NPs may exert adverse effects by excessively stimulating or disrupting normal cellular processes that can lead to cytotoxicity.[69] Polyphenol-capped NPs have been shown to decrease toxicity and improve cellular tolerance.[68] Both NPs in this study possess an organic outer coating of poly(allylamine hydrochloride) (PAH). Additionally, TA-SeNPs contain organic compounds derived from the TA extract of plant origin. Hence, it is essential to identify whether they can cause cytotoxicity by stimulating non-specific responses. Therefore, the effects of the TA extract,

SeNPs, and TA-SeNPs were analyzed at various concentrations on fibroblasts to assess the cell viability and metabolic activity.

The TA extract showed no impact on cell metabolism after 72 h. However, both SeNPs and TA-SeNPs caused a time and dose-dependent reduction in cell viability. Significant decreases were observed at 48 h and 72 h for both types of NPs with the two highest doses. The enhanced biocompatibility of TA-SeNPs may be attributed to the antioxidative and stabilizing effects of the TA extract, which reduced oxidative stress and influence cellular uptake, leading to lower cytotoxicity in iNHDF-1. These findings aligned with a previous study by Zhang *et al.*,[70] which reported that polyphenol-capped NPs showed decreased toxicity and improved cellular tolerance.

The findings of $IC_{50}$ show that both NPs exhibit size-, dose-, and time-dependent cytotoxic effects on cells. TA-SeNPs showed a lower $IC_{50}$ value compared to SeNPs at 72 h, suggesting enhanced bioactivity possibly due to the synergistic effect of tannic acid capping. This indicates that TA functionalization may improve the NP–cell interaction or uptake, contributing to increased cytotoxic potential over time. This improved biocompatibility of TA-SeNPs may be attributed to the antioxidative and stabilizing effects of the TA extract, which reduces oxidative stress and influences cellular uptake, leading to lower cytotoxicity. Several studies have reported no cytotoxicity following exposure to biogenic SeNPs, including *Yarrowia lipolytica*-produced biogenic SeNPs[42] and Gram-negative (*Stenotrophomonas maltophilia*) bacteria- and Gram-positive (*Bacillus mycoides*) bacteria-derived biogenic SeNPs,[69] while other studies have observed cytotoxic effects even at low concentrations of biogenic SeNPs.[71] Similarly, the studies cited in refs. 69 and 72 reported no significant effect compared to the untreated control groups for the chemically produced SeNPs.

We performed several control experiments to verify the role of the TA extract in NP synthesis and antioxidant activity. The UV–visible spectra of $Na_2SeO_3$ alone initially showed no visible absorption peak, while those of the TA extract showed a broad absorption band attributed to the various phytochemicals present in the TA extract, indicating that both are necessary components for TA-SeNP formation. Fourier transform infrared (FTIR) spectroscopy analysis of the TA extract showed functional groups capable of reducing and stabilizing the NPs. Furthermore, the TA extract was also tested independently in *in vitro* chemical antioxidant assays (FRAP, DPPH, $H_2O_2$, superoxide, and NO scavenging assays), as well as in a cell viability assay using human dermal fibroblasts, signifying the biocompatibility and antioxidant activity. These results validate the NP formation and that the subsequent intracellular ROS scavenging activity of TA-SeNPs occur due to the combined activity of the precursor and bioactive components of the TA extract.

Furthermore, the intracellular antioxidant-mediated protective effects of both NPs were determined by measuring the ROS levels in human dermal fibroblasts under $H_2O_2$-induced oxidative stress using ROS scavenging and DCFH-DA assays. Both NPs exhibited greater ROS scavenging activity than AA, indicating the protective effects of NPs. A strong ROS-scavenging effect has been reported for ultrasmall biogenic SeNPs

derived from Hericium erinaceus polysaccharides.[40] Surface modification with hyaluronic acid SeNPs does not, interestingly, seem to prevent effective reduction of ROS levels.[73,74]

## 5. Conclusions

Biogenic synthesis provides a sustainable, cost-effective, and eco-friendly approach to produce small-sized *Trachyspermum ammi* (TA)-selenium nanoparticles (SeNPs) (TA-SeNPs) with enhanced biocompatibility and significantly greater antioxidant activity compared to their chemically synthesized counterparts. Our results show that TA-SeNPs exhibit good physicochemical and biological properties, positioning them as promising candidates for biomedical applications, especially in antioxidant and immune modulation therapies. The small-sized antioxidant NPs may enable new therapeutic applications where improved tissue penetration is needed.

## Author contributions

Naila Qamar: conceptualization, methodology, investigation, validation, formal analysis, funding, and writing – original draft. Milka Poimala, Jiri Jäntti, Shuvashis Das Gupta, and Ayman Hawash: methodology, investigation, validation, and writing – review & editing. Charith Sandipa Leelarathne: resources and writing – review & editing. Daniela Mennerich: resources, methodology, and writing – review & editing. Antoine Dufour: supervision, project administration, and writing – review & editing. Janne Mäkelä: resources, project administration, and writing – review & editing. Pirjo Åström and Mikko A.J. Finnilä: conceptualization, methodology, resources, supervision, project administration, funding acquisition, and writing – review & editing.

## Conflicts of interest

The authors have no competing personal or financial interest to declare.

## Data availability

The data that support the findings of this study can be obtained from the corresponding author upon reasonable request.

Supplementary information (SI) is available. Full experimental details, protocols, reagent concentrations, and calculation formulae. See DOI: https://doi.org/10.1039/d5bm01855b.

## Acknowledgements

## References

1 D. S. Chormey, B. T. Zaman, T. Borahan Kustanto, S. Erarpat Bodur, S. Bodur, Z. Tekin, *et al.*, Biogenic synthesis of novel nanomaterials and their applications, *Nanoscale*, 2023, **15**, 19423–19447, DOI: 10.1039/D3NR03843B.

2 B. Mughal, S. Z. J. Zaidi, X. Zhang and S. U. Hassan, Biogenic Nanoparticles: Synthesis, Characterisation and Applications, *Appl. Sci.*, 2021, **11**(6), 2598, DOI: 10.3390/APP11062598.

3 S. Bayda, M. Adeel, T. Tuccinardi, M. Cordani and F. Rizzolio, The History of Nanoscience and Nanotechnology: From Chemical–Physical Applications to Nanomedicine, *Molecules*, 2019, **25**, 112, DOI: 10.3390/MOLECULES25010112.

4 U. Laila, M. Akram, F. S. Khan, F. A. Ozdemir and I. J. Umaru, Understanding Modern Nanotechnology: Insights into Its Evolution, Applications, and Global Impact, *Kwaghe Int. J. Sci. Technol.*, 2025, **2**, 279–286, DOI: 10.58578/KIJST.V2I2.6622.

5 M. Shakibaie, A. R. Shahverdi, M. A. Faramarzi, G. R. Hassanzadeh, H. R. Rahimi and O. Sabzevari, Acute and subacute toxicity of novel biogenic selenium nanoparticles in mice, *Pharm. Biol.*, 2013, **51**, 58–63, DOI: 10.3109/13880209.2012.710241.

6 A. Bhattacharjee, A. Basu, P. Ghosh, J. Biswas and S. Bhattacharya, Protective effect of Selenium nanoparticle against cyclophosphamide induced hepatotoxicity and genotoxicity in Swiss albino mice, *J. Biomater. Appl.*, 2014, **29**, 303–317, DOI: 10.1177/0885328214523323.

7 E. O. Mikhailova, Selenium Nanoparticles: Green Synthesis and Biomedical Application, *Molecules*, 2023, **28**, 8125, DOI: 10.3390/MOLECULES28248125.

8 C. Zhai, Y. Lin, C. Mao, X. Li, R. Zhang, J. Liu, *et al.*, Construction, characterization, antioxidant activity and effects on properties in vitro digestion of selenium nanoparticles decorated with Cyperus esculentus polysaccharides, *Food Biosci.*, 2024, **59**, 104062, DOI: 10.1016/J.FBIO.2024.104062.

9 M. A. O. Dawood, M. F. El Basuini, S. Yilmaz, H. M. R. Abdel-Latif, Z. A. Kari, M. K. A. Abdul Razab, *et al.*, Selenium Nanoparticles as a Natural Antioxidant and Metabolic Regulator in Aquaculture: A Review, *Antioxidants*, 2021, **10**, 1364, DOI: 10.3390/ANTIOX10091364.

10 E. O. Mikhailova, Selenium Nanoparticles: Green Synthesis and Biomedical Application, *Molecules*, 2023, **28**, 8125, DOI: 10.3390/MOLECULES28248125.

11 U. Tinggi, Selenium: its role as antioxidant in human health, *Environ. Health Prev. Med.*, 2008, **13**, 102–108, DOI: 10.1007/S12199-007-0019-4.

12 Y. Zhang, L. Chen, R. Sun, R. Lv, T. Du, Y. Li, *et al.*, Multienzymatic Antioxidant Activity of Manganese-Based Nanoparticles for Protection against Oxidative Cell Damage, *ACS Biomater. Sci. Eng.*, 2022, **8**, 638–648, DOI: 10.1021/ACSBIOMATERIALS.1C01286/ASSET/IMAGES/LARGE/AB1C01286_0008.JPEG.

13 N. Singh, M. A. Savanur, S. Srivastava, P. D′silva and G. Mugesh, A manganese oxide nanozyme prevents the oxidative damage of biomolecules without affecting the endogenous antioxidant system, *Nanoscale*, 2019, **11**, 3855, DOI: 10.1039/c8nr09397k.

14 M. Y. Ansari, N. Ahmad and T. M. Haqqi, Oxidative stress and inflammation in osteoarthritis pathogenesis: Role of polyphenols, *Biomed. Pharmacother.*, 2020, **129**, 110452, DOI: 10.1016/J.BIOPHA.2020.110452.

15 S. Ye, F. Liu, J. Wang, H. Wang and M. Zhang, Antioxidant activities of an exopolysaccharide isolated and purified from marine Pseudomonas PF-6, *Carbohydr. Polym.*, 2012, **87**, 764–770, DOI: 10.1016/J.CARBPOL.2011.08.057.

16 S. A. Wadhwani, U. U. Shedbalkar, R. Singh and B. A. Chopade, Biogenic selenium nanoparticles: current status and future prospects, *Appl. Microbiol. Biotechnol.*, 2016, **100**, 2555–2566, DOI: 10.1007/S00253-016-7300-7/FIGURES/3.

17 A. H. Al-Wakeel, S. Elbahnaswy, E. A. Eldessouki, E. Risha and E. Zahran, Dietary biogenic selenium nanoparticles improve growth and immune-antioxidant indices without inducing inflammatory responses in Nile tilapia, *Sci. Rep.*, 2024, **14**, 21990, DOI: 10.1038/s41598-024-72022-w.

18 M. M. El-Zahed, S. A. Kandel and M. E. Khalifa, Antiviral activity of green synthesized selenium nanoparticles alone and in combination with chitosan against SARS-CoV-2, *Discover Nano*, 2026, **21**, 12, DOI: 10.1186/s11671-025-04420-6.

19 A. S. Alhawiti, Citric acid-mediated green synthesis of selenium nanoparticles: antioxidant, antimicrobial, and anticoagulant potential applications, *Biomass Convers. Biorefin.*, 2024, **14**, 6581–6590, DOI: 10.1007/s13399-022-02798-2.

20 P. Liu, H. Long, H. Cheng, M. Liang, Z. Liu, Z. Han, *et al.*, Highly-efficient synthesis of biogenic selenium nanoparticles by Bacillus paramycoides and their antibacterial and antioxidant activities, *Front. Bioeng. Biotechnol.*, 2023, **11**, 1227619, DOI: 10.3389/fbioe.2023.1227619.

21 A. Ullah, X. Yin, F. Wang, B. Xu, Z. A. Mirani, B. Xu, M. W. H. Chan, A. Ali, M. Usman, N. Ali and M. Naveed, Biosynthesis of Selenium Nanoparticles (via *Bacillus subtilis* BSN313), and Their Isolation, Characterization, and Bioactivities, *Molecules*, 2021, **26**(18), 5559, DOI: 10.3390/molecules26185559.

22 S. Pandey, N. Awasthee, A. Shekher, L. C. Rai, S. C. Gupta and S. K. Dubey, Biogenic synthesis and characterization of selenium nanoparticles and their applications with special reference to antibacterial, antioxidant, anticancer and photocatalytic activity, *Bioprocess Biosyst. Eng.*, 2021, **44**, 2679–2696, DOI: 10.1007/s00449-021-02637-0.

23 S. Y. S. Zeebaree, A. Y. S. Zeebaree and O. I. H. Zebari, Diagnosis of the multiple effect of selenium nanoparticles decorated by Asteriscus graveolens components in inhibiting HepG2 cell proliferation, *Sustainable Chem. Pharm.*, 2020, **15**, 100210, DOI: 10.1016/j.scp.2019.100210.

24 K. Anu, S. Devanesan, R. Prasanth, M. S. AlSalhi, S. Ajithkumar, G. Singaravelu, *et al.*, Biogenesis of selenium nanoparticles and their anti-leukemia activity, *J. King Saud Univ., Sci.*, 2020, **32**, 2520–2526, DOI: 10.1016/j.jksus.2020.04.018.

25 S. Menon, S. D. Shrudhi, H. Agarwal and V. K. Shanmugam, Efficacy of Biogenic Selenium Nanoparticles from an Extract of Ginger towards Evaluation on Anti-Microbial and Anti-Oxidant Activities, *Colloid Interface Sci. Commun.*, 2019, **29**, 1–8, DOI: 10.1016/j.colcom.2018.12.004.

26 V. Alagesan and S. Venugopal, Green Synthesis of Selenium Nanoparticle Using Leaves Extract of Withania somnifera and Its Biological Applications and Photocatalytic Activities, *BioNanoScience*, 2018, **9**, 105–116, DOI: 10.1007/s12668-018-0566-8.

27 A. Arif, A. Bhatti and P. John, Therapeutic Potential Of Foeniculum vulgare Mill. Derived Selenium Nanoparticles In Arthritic Balb/c Mice, *Int. J. Nanomed.*, 2019, **14**, 8561–8572, DOI: 10.2147/IJN.S226674.

28 N. Qamar, P. John and A. Bhatti, Toxicological and Anti-Rheumatic Potential of Trachyspermum ammi Derived Biogenic Selenium Nanoparticles in Arthritic Balb/c Mice, *Int. J. Nanomed.*, 2020, **15**, 3497–3509, DOI: 10.2147/IJN.S243718.

29 V. K. Bajpai, Y. H. Park and P. Agrawal, Studies on phytochemical analysis, antioxidant and lipid peroxidation inhibitory effects of a medicinal plant, Coleus forskohlii, *Front. Life Sci.*, 2015, **8**, 139–147, DOI: 10.1080/21553769.2014.998777.

30 U. Saleem, S. Riaz, B. Ahmad and S. Mohammad, Pharmacological Screening of Trachyspermum ammi for Antihyperlipidemic Activity in Triton X-100 Induced Hyperlipidemia Rat Model, *Pharmacogn. Res.*, 2017, **9**, S34–S40, DOI: 10.4103/PR.PR_37_17.

31 R. Bairwa, R. S. Sodha and B. S. Rajawat, Trachyspermum ammi, *Pharmacogn. Rev.*, 2012, **6**, 56–60, DOI: 10.4103/0973-7847.95871.

32 S. Umar, M. Asif, M. Sajad, M. Ansari, U. Hussain, W. Ahmad, *et al.*, Anti-inflammatory and antioxidant activity of Trachyspermum ammi seeds in collagen induced arthritis in rats, *Int. J. Drug Dev. Res.*, 2012, **4**, 210–219.

33 K. Perveen, F. M. Husain, F. A. Qais, A. Khan, S. Razak, T. Afsar, *et al.*, Microwave-Assisted Rapid Green Synthesis of Gold Nanoparticles Using Seed Extract of Trachyspermum ammi: ROS Mediated Biofilm Inhibition and Anticancer Activity, *Biomolecules*, 2021, **11**, 197, DOI: 10.3390/BIOM11020197.

34 S. Vk, R. Subashini, A. Israel, K. Murugan and N. Ramakrishnan, Trachyspermum ammi seed extract-

mediated Ag nanoparticles: an insight into its in vitro biopotency, *Biomass Convers. Biorefin.*, 2025, **15**, 313–326, DOI: 10.1007/S13399-023-04976-2/FIGURES/16.

35 B. D. Sethuraman, L. P. Chandrasekar, M. Subramani and S. Mohandos, Trachyspermum ammi Mediated Green Synthesis of NiO Nanoparticles: Dual Role in Photocatalytic Degradation and Anti-bacterial Efficacy, *Int. J. Environ. Anal. Chem.*, 2025, **105**, 5062–5082, DOI: 10.1080/03067319.2024.2383972;WGROUP:STRING:PUBLICATION.

36 A. Bagherivand, S. Jafarirad, R. Norouzi, E. Rezazadeh and A. Karimi, Zinc oxide/barite nanocomposite from Trachyspermum ammi plant extract: A novel agent against protoscolices of Echinococcus granulosus, *J. Drug Delivery Sci. Technol.*, 2024, **100**, 106024, DOI: 10.1016/J.JDDST.2024.106024.

37 R. Prakash, N. Gupta, N. Sharma, V. Kumar and W. Adnew, Biomedical and industrial applications of Trachyspermum ammi-derived nanoparticles: a comprehensive review, *Discover Nano*, 2026, **21**, 10, DOI: 10.1186/S11671-026-04436-6.

38 S. Ahmad, M. A. Ahmad, N. Ahmad, M. S. Islam, A. Rauf, S. ERCİŞLİ, M. S. Elshikh, M. S. Alwahibi, R. Iqbal and M. Lackner, Effects Of Trachyspermum Ammi Leaf-Synthesized Zinc Oxide Nanoparticles On Germination, Early Seedling Growth And Biomass Of Various Rice Varieties, *Appl. Ecol. Environ. Res.*, 2025, **23**, 6373–6389, DOI: 10.15666/aeer/2304_63736389.

39 S. Malhotra, M. N. Welling, S. B. Mantri and K. Desai, *In vitro* and *in vivo* antioxidant, cytotoxic, and anti-chronic inflammatory arthritic effect of selenium nanoparticles, *J. Biomed. Mater. Res., Part B*, 2016, **104**, 993–1003, DOI: 10.1002/jbm.b.33448.

40 H. He, C. Liu, C. Shao, Y. Wu and Q. Huang, Green synthesis of ultrasmall selenium nanoparticles (SeNPs) using Hericium erinaceus polysaccharide (HEP) as nanozymes for efficient intracellular antioxidation, *Mater. Lett.*, 2022, **317**, 132079, DOI: 10.1016/J.MATLET.2022.132079.

41 W. Majeed, M. Zafar, A. Bhatti and P. John, Therapeutic Potential of Selenium Nanoparticles, *J. Nanomed. Nanotechnol.*, 2018, **09**, 1, DOI: 10.4172/2157-7439.1000487.

42 E. Lashani, H. Moghimi, R. J. Turner and M. A. Amoozegar, Characterization and biological activity of selenium nanoparticles biosynthesized by Yarrowia lipolytica, *Microb. Biotechnol.*, 2024, **17**, e70013, DOI: 10.1111/1751-7915.70013.

43 O. Ibraheem, O. H. Oyeniran, O. M. Ogundipe, E. O. Abe, T. A. Oyedepo, K. O. Sodeinde, S. O. Damola and T. B. Adeola, Photo-physical characterizations and evaluation of *in vitro* antioxidant, anti-inflammatory and antidiabetic potentials of green synthesized ackee (Blighia sapida), *BMC Complementary Med. Ther.*, 2024, **24**, 392, DOI: 10.1186/s12906-024-04694-w.

44 M. Vahdati and T. Tohidi Moghadam, Synthesis and Characterization of Selenium Nanoparticles-Lysozyme Nanohybrid System with Synergistic Antibacterial Properties, *Sci. Rep.*, 2020, **10**, 1–10, DOI: 10.1038/s41598-019-57333-7.

45 S. Vasanthakumar, M. Manikandan and M. Arumugam, Green synthesis, characterization and functional validation of bio-transformed selenium nanoparticles, *Biochem. Biophys. Rep.*, 2024, **39**, 101760, DOI: 10.1016/J.BBREP.2024.101760.

46 E. Sans-Serramitjana, C. Gallardo-Benavente, F. Melo, J. M. Pérez-Donoso, C. Rumpel, P. J. Barra, P. Durán and M. D. Mora, A comparative study of the synthesis and characterization of biogenic selenium nanoparticles by two contrasting endophytic selenobacteria, *Microorganisms*, 2023, **11**, 1600, DOI: 10.3390/microorganisms11061600.

47 D. Cord, M. C. Rîmbu, M. P. Iordache, R. Albulescu, S. Pop, C. Tanase and M. L. Popa, Phytochemicals as Epigenetic Modulators in Chronic Diseases: Molecular Mechanisms, *Molecules*, 2025, **30**, 4317, DOI: 10.3390/MOLECULES30214317.

48 P. Rajkumar, S. Selvaraj, R. Suganya, D. Velmurugan, S. Gunasekaran and S. Kumaresan, Vibrational and electronic spectral analysis of thymol an isomer of carvacrol isolated from Trachyspermum ammi seed: A combined experimental and theoretical study, *Chem. Data Collect.*, 2018, **15–16**, 10–31, DOI: 10.1016/J.CDC.2018.03.003.

49 C. O. Akoto, A. Acheampong, Y. Duah Boakye, B. K. Kokloku, G. Kwarteng and B. Kwadzo Kokloku, In vitro anthelmintic, anti-inflammatory, antioxidant activities and FTIR analysis of Sclerocarya birrea root, *J. Pharmacogn. Phytochem.*, 2020, **9**, 1389–1401, https://api.semanticscholar.org/CorpusID:221759792.

50 B. E. F. Elsaied, A. M. Diab, A. A. Tayel, M. A. Alghuthaymi and S. H. Moussa, Potent antibacterial action of phyco-synthesized selenium nanoparticles using Spirulina platensis extract, *Green Process. Synth.*, 2021, **10**, 49–60, DOI: 10.1515/GPS-2021-0005/ASSET/GRAPHIC/J_GPS-2021-0005_FIG_007.JPG.

51 K. Brindhadevi, S. Vasantharaj, Q. H. Le, S. Devanesan, K. Farhat and X. Liu, Fabrication and characterization of manganese dioxide ($MnO_2$) nanoparticles and its degradation potential of benzene and pyrene, *Chemosphere*, 2023, **343**, 140123, DOI: 10.1016/J.CHEMOSPHERE.2023.140123.

52 S. Qin, X. Liu, W. Lv, J. Hu, X. Huang and L. Zhao, The mechanism of degradation polycyclic aromatic hydrocarbons by magnetic biogenic manganese oxides, *Biochem. Eng. J.*, 2023, **191**, 108803, DOI: 10.1016/J.BEJ.2022.108803.

53 S. A. Moon, B. K. Salunke, B. Alkotaini, E. Sathiyamoorthi and S. Kim, Biological synthesis of manganese dioxide nanoparticles by Kalopanax pictus plant extract, *IET Nanobiotechnol.*, 2015, **9**, 220–225, DOI: 10.1049/iet-nbt.2014.0051.

54 A. Arif, A. Bhatti and P. John, Therapeutic potential of Foeniculum vulgare mill. Derived selenium nanoparticles in arthritic Balb/c mice, *Int. J. Nanomed.*, 2019, **14**, 8561–8572, DOI: 10.2147/IJN.S226674.

55 A. J. Kora and L. Rastogi, Biomimetic synthesis of selenium nanoparticles by Pseudomonas aeruginosa ATCC 27853: An

approach for conversion of selenite, *J. Environ. Manage.*, 2016, **181**, 231–236, DOI: 10.1016/j.jenvman.2016.06.029.

56 S. Lampis, E. Zonaro, C. Bertolini, P. Bernardi, C. S. Butler and G. Vallini, Delayed formation of zero-valent selenium nanoparticles by Bacillus mycoides SeITE01 as a consequence of selenite reduction under aerobic conditions, *Microb. Cell Fact.*, 2014, **13**, 1–14, DOI: 10.1186/1475-2859-13-35.

57 K. Spyridopoulou, E. Tryfonopoulou, G. Aindelis, P. Ypsilantis, C. Sarafidis, O. Kalogirou and K. Chlichlia, Biogenic selenium nanoparticles produced by Lactobacillus casei ATCC 393 inhibit colon cancer cell growth in vitro and in vivo, *Nanoscale Adv.*, 2021, **3**, 2516–2528, DOI: 10.1039/d0na00984a.

58 D. N. Nagar, N. N. Ghosh and J. M. Braganca, Green synthesis of selenium nanospheres and nanoneedles by halophilic archaea, *Appl. Nanosci.*, 2022, **12**, 3983–3994, DOI: 10.1007/S13204-022-02665-6/FIGURES/10.

59 E. Haro-Poniatowski, L. Escobar-Alarcón, J. L. Hernández-Pozos, L. G. Mendoza-Luna and C. A. Guarin, Synthesis and characterization of selenium nanoparticles obtained by femtosecond pulsed laser ablation in liquid media, *Appl. Phys. A:Mater. Sci. Process.*, 2022, **128**, 1–7, DOI: 10.1007/S00339-022-05956-5/FIGURES/5.

60 S. N. Yannopoulos and K. S. Andrikopoulos, Raman scattering study on structural and dynamical features of noncrystalline selenium, *J. Chem. Phys.*, 2004, **121**, 4747–4758, DOI: 10.1063/1.1780151.

61 S. Chaudhary and S. K. Mehta, Selenium Nanomaterials: Applications in Electronics, Catalysis and Sensors, *J. Nanosci. Nanotechnol.*, 2014, **14**, 1658–1674, DOI: 10.1166/JNN.2014.9128.

62 A. V. Tugarova, P. V. Mamchenkova, Y. A. Dyatlova and A. A. Kamnev, FTIR and Raman spectroscopic studies of selenium nanoparticles synthesised by the bacterium Azospirillum thiophilum, *Spectrochim. Acta, Part A*, 2018, **192**, 458–463, DOI: 10.1016/J.SAA.2017.11.050.

63 F. A. Akçay and A. Avcı, Effects of process conditions and yeast extract on the synthesis of selenium nanoparticles by a novel indigenous isolate Bacillus sp. EKT1 and characterization of nanoparticles, *Arch. Microbiol.*, 2020, **202**, 2233–2243, DOI: 10.1007/S00203-020-01942-8.

64 S. Ramya, T. Shanmugasundaram and R. Balagurunathan, Biomedical potential of actinobacterially synthesized selenium nanoparticles with special reference to anti-biofilm, anti-oxidant, wound healing, cytotoxic and anti-viral activities, *J. Trace Elem. Med. Biol.*, 2015, **32**, 30–39, DOI: 10.1016/J.JTEMB.2015.05.005.

65 K. Wei, X. Yin, F. Chen, X. Wang, W. Ding and B. Ding, Synthesis, characterization, and bioactivity of selenium nanoparticles stabilized by regenerated chitin nanofibers, *Int. J. Biol. Macromol.*, 2025, **309**, 142791, DOI: 10.1016/J.IJBIOMAC.2025.142791.

66 O. Blokhina, E. Virolainen and K. V. Fagerstedt, Antioxidants, Oxidative Damage and Oxygen Deprivation Stress: a Review, *Ann. Bot.*, 2003, **91**, 179–194, DOI: 10.1093/AOB/MCF118.

67 M. Yazhiniprabha and B. Vaseeharan, In vitro and in vivo toxicity assessment of selenium nanoparticles with significant larvicidal and bacteriostatic properties, *Mater. Sci. Eng., C*, 2019, **103**, 109763, DOI: 10.1016/J.MSEC.2019.109763.

68 B. Afzal, D. Yasin, H. Naaz, N. Sami, A. Zaki, M. A. Rizvi, *et al.*, Biomedical potential of Anabaena variabilis NCCU-441 based Selenium nanoparticles and their comparison with commercial nanoparticles, *Sci. Rep.*, 2021, **11**, 1–15, DOI: 10.1038/s41598-021-91738-7.

69 E. Cremonini, E. Zonaro, M. Donini, S. Lampis, M. Boaretti, S. Dusi, *et al.*, Biogenic selenium nanoparticles: characterization, antimicrobial activity and effects on human dendritic cells and fibroblasts, *Microb. Biotechnol.*, 2016, **9**, 758–771, DOI: 10.1111/1751-7915.12374.

70 Z. Zhang, W. Sang, L. Xie, W. Li, B. Li, J. Li, *et al.*, Polyphenol-Based Nanomedicine Evokes Immune Activation for Combination Cancer Treatment, *Angew. Chem., Int. Ed.*, 2021, **60**, 1967–1975, DOI: 10.1002/ANIE.202013406.

71 C. Xu, L. Qiao, Y. Guo, L. Ma and Y. Cheng, Preparation, characteristics and antioxidant activity of polysaccharides and proteins-capped selenium nanoparticles synthesized by Lactobacillus casei ATCC 393, *Carbohydr. Polym.*, 2018, **195**, 576–585, DOI: 10.1016/J.CARBPOL.2018.04.110.

72 M. Guo, Y. Li, Z. Lin, M. Zhao, M. Xiao, C. Wang, *et al.*, Surface decoration of selenium nanoparticles with curcumin induced HepG2 cell apoptosis through ROS mediated p53 and AKT signaling pathways, *RSC Adv.*, 2017, **7**, 52456–52464, DOI: 10.1039/C7RA08796A.

73 Y. Li, S. Zhu, J. Luo, Y. Tong, Y. Zheng, L. Ji, *et al.*, The Protective Effect of Selenium Nanoparticles in Osteoarthritis: In vitro and in vivo Studies, *Drug Des., Dev. Ther.*, 2023, **17**, 1515–1529, DOI: 10.2147/DDDT.S407122.

74 C. Liu, W. Du, L. Zhang and J. Wang, Natural synergy: Oleanolic acid-curcumin co-assembled nanoparticles combat osteoarthritis, *Colloids Surf., B*, 2025, **245**, 114286, DOI: 10.1016/j.colsurfb.2024.114286.